Insights into Vapor-Liquid Equilibrium of Lennard–Jones systems via Computational Modeling

A Thesis

submitted to

Indian Institute of Science Education and Research Pune

in partial fulfillment of the requirements for the

Master's Degree Programme

by

Saurabh Singh

Indian Institute of Science Education and Research Pune
Dr. Homi Bhabha Road,
Pashan, Pune 411008, INDIA.

April, 2026

Supervisor: **Dr. Arnab Mukherjee**

Certificate

This is to certify that this project entitled **”Insights into Vapor-Liquid Equilibrium of Lennard–Jones systems via Computational Modeling”** in partial fulfillment of the Master’s program at the Indian Institute of Science Education and Research, Pune represents original research work carried out by Saurabh Singh at IISER Pune under the supervision of **Dr. Arnab Mukherjee**, Professor, IISER Pune during the academic year **2025-2026**.

Arnab Mukherji

Dr. Arnab Mukherjee

Committee:

Dr. Arnab Mukherjee

Dr. Anirban Hazra

This thesis is dedicated to...

My Parents

Declaration

I hereby declare that the matter embodied in the report entitled **”Insights into Vapor-Liquid Equilibrium of Lennard–Jones systems via Computational Modeling”** are the results of the work carried out by me at the Department of Chemistry, Indian Institute of Science Education & Research (IISER) Pune, under the supervision of **Dr. Arnab Mukherjee**, and the same has not been submitted elsewhere for any other degree. Wherever others contribute, every effort is made to indicate this clearly, with due reference to the literature and acknowledgement of collaborative research and discussions.

SSingh

Date: 23-03-2026
Pune (MH), India

Saurabh Singh
(20246212)

Acknowledgement

I would like to express my sincere gratitude to my supervisor, **Dr. Arnab Mukherjee**, for his constant guidance, encouragement, and insightful suggestions throughout the course of this research. His support and perspective have been invaluable in shaping this work.

I am especially thankful to my mentor, **Mr. Parth Joshi**, for his continuous support, guidance, and for many meaningful discussions that greatly contributed to the development of this study.

I would also like to acknowledge **Mr. Bikirna Roy** and **Mr. Ashish Kumar** for their assistance, helpful suggestions, and for sharing their knowledge during the course of this work.

I am grateful to my expert committee member, **Dr. Anirban Hazra**, for his valuable feedback and constructive suggestions, which have helped improve the quality of this thesis.

I also thank my labmates and colleagues for fostering a supportive and collaborative environment.

Finally, I express my heartfelt gratitude to my family for their unwavering support, patience, and encouragement throughout my academic journey.

Contents

List of Figures

List of Tables

Abstract

Azeotropes are special mixtures in which the components have same composition both in liquid and vapor phases at a specific temperature and pressure. Because of this property, the two components act as a single liquid and boil together, making separation difficult. This study is important for improving separation process in physical chemistry. However, the prediction of azeotropic shift remains challenging due to competing molecular factors. For the study of this behaviour, molecular dynamics simulations are performed using GROMACS. The vapor-liquid equilibrium of binary Lennard-Jones (LJ) mixtures is studied to understand the effects of temperature, composition, and asymmetry in interaction or size on phase behavior. The simulations were conducted in the range of compositions (χ_A = 0.1 to 0.9) and temperatures (60 K, 80 K, 100 K, and 120 K) for symmetric mixture (single component system) and asymmetric mixtures that have differences in the strength of interaction (ϵ) and molecular size (σ). Number density profiles, radial distribution functions (RDF), mole fraction vs. composition analysis, and interfacial analysis were used to study the structural and compositional properties of binary mixtures. The profiles of the number density showed that there was a clear separation between the vapor and the liquid phase, with a decrease in the density variations with an increase in the temperature. The RDF analysis indicated the existence of short-range ordering in the liquid phase, which decreased with high temperature. The compositional analysis showed the change in the concentration of each component with the overall mole fraction, whereas the interfacial analysis revealed the nature of the transition region between the vapor and liquid phases.

This study shows that asymmetric interactions play a major role in the shift of the azeotropic point. These findings provide better insight into the molecular interactions that regulate the vapor-liquid equilibrium and provide information about azeotrope formation.

The study was extended to a real system by investigating the vapor–liquid equilibrium of the benzene–methanol azeotrope using the AMOEBA force field; however, reliable results could not be obtained due to difficulties in achieving stable pressure equilibration. In future work, more advanced machine learning potentials will be explored to improve the accuracy and efficiency of the molecular simulations.

1 Introduction

Solutions are an essential part of many chemical systems, and their behavior is strongly dependent on how the different components interact with each other. Based on these interactions, solutions are commonly classified as ideal and non-ideal solutions. This classification helps to understand the mixing behavior, phase equilibrium, and thermodynamic properties of real systems.

An ideal solution is a mixture in which all molecules interact in a similar manner, regardless of whether they belong to the same substance or to different components. In such systems, the interactions between like molecules are nearly identical to those between unlike molecules. Because of this similarity, mixing occurs smoothly without any noticeable structural or energetic changes. These solutions follow Raoult's law, and benzene–toluene or n-hexane–n-heptane are such examples of these solutions.

1.1 Azeotrope

An azeotrope is a mixture of two or more components that has a constant boiling point and the same composition in both the liquid and the vapor phase.[2] Exhibits this special property that makes separation difficult. Advanced distillation techniques, such as azeotropic distillation,[3] extractive distillation,[4] and pressure-swing distillations,[5] are commonly used to separate azeotropic mixtures. Azeotropic distillation involves the addition of a third component (an entrainer) to alter the relative volatility of the components to break the azeotrope. Pressure-swing distillation uses changes in pressure to shift the azeotropic composition, allowing separation at different pressures. Extractive distillation is another method in which a solvent is introduced to change intermolecular interactions and improve separation efficiency. Azeotropes have significant importance in the chemical industry.[6] They help minimize waste in industrial processes.[7] They are used as fuel blends to improve engine performance by adjusting boiling points and compositions,[8][9] and serve as sustainable multipurpose solvents in vapor-phase cleaning applications.[10][11]

Thermodynamically, a binary mixture is classified as an azeotrope when it satisfies the following condition:

$$x_i^l = x_i^v \tag{1}$$

where x_i^l and x_i^v represent the mole fractions of component i in the liquid and vapor phases, respectively. Equation 1 represents that the mole fraction of component i in the liquid phase and in the vapor phase must be the same.[12]

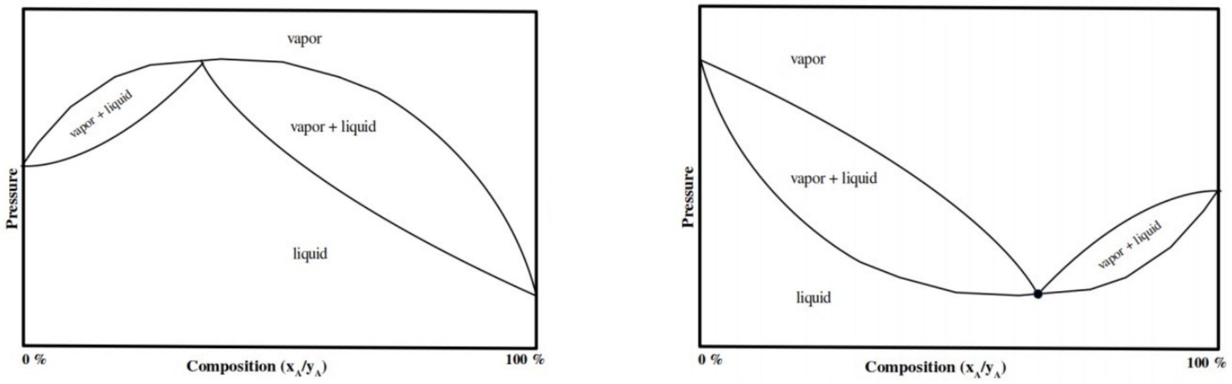

(a) Positive azeotrope

(b) Negative azeotrope

Figure 1: Pressure–composition phase diagrams showing (a) positive (minimum boiling) azeotrope (b) negative (maximum boiling) azeotrope.[1]

Azeotropes are classified into positive (minimum boiling) and negative (maximum boiling) azeotropes based on their deviation from Raoult's law (deviation of vapour pressure w.r.t. mole fraction) and boiling point behavior. Raoult's law describes the equilibrium behavior of the liquid-vapor of an ideal liquid mixture. It states that, at a fixed temperature, the partial vapor pressure of each component in a mixture is directly proportional to its mole fraction in the liquid phase.[13] And the total vapor pressure is equal to the sum of the partial pressures of all components.[14]

$$y_i P = x_i P_i^{\text{sat}} \tag{2}$$

$$P = x_1 P_1^{\text{sat}} + x_2 P_2^{\text{sat}} \tag{3}$$

$$P = \sum_{i=1}^{n} x_i P_i^{\text{sat}} \tag{4}$$

where x_i and y_i represent the mole fractions of component i in the liquid and vapor phases, respectively, P_i^{sat} is the saturation vapor pressure of component i, and P is the total pressure of the system.

1.2 Vapor Liquid Equilibrium (VLE)

Vapor-liquid equilibrium describes the condition of simultaneous existence of a liquid phase and a vapor phase with no net transfer of matter between the two. VLE results in the same rates of evaporation and condensation and therefore results in constant thermodynamic values (temperature, pressure, and phase composition). VLE is important for understanding the phase changes and the thermodynamic stability of liquid systems. To maintain the thermodynamic viability of both phases within the equilibrium state, the chemical potential of each component must be equal to that of the other phase as given by the equation 5:

$$\mu_i^{(l)} = \mu_i^{(v)} \tag{5}$$

In addition to the properties of each component, intermolecular forces as well as external factors (temperature and pressure) determine the relative distribution of molecules between the vapor and liquid phases. As the temperature of a liquid increases, so does the kinetic energy of the molecules, thus allowing more molecules to escape to the vapor phase, thereby increasing the amount of vapor formed.

Vapor-liquid coexistence studies are significant in the discipline of molecular simulation because fluid properties are modeled with simplified intermolecular potentials. Understanding how interactions among molecules affect observable characteristics such as density, temperature, and composition helps to better characterize the thermodynamics and interfacial structure of a system and to study phase behavior in fluids in general.

1.3 Force Fields

Force fields describe the interactions between atoms in molecular systems. They are broadly classified into polarizable[15] and non-polarizable force fields. Polarizable force fields allow atomic charge distributions to respond dynamically to the local electric field through induced dipoles.[15] In non-polarizable force fields, including OPLS,[16] CHARMM,[17] AMBER,[18] GROMOS,[19] and TraPPE-UA,[20] atomic partial charges are fixed throughout the simulation. Due to their lower computational cost and numerical stability, non-polarizable force fields are suitable for large systems and long simulation times.

1.4 Objective

This study focuses on understanding vapor–liquid equilibrium (VLE) using a Lennard–Jones binary mixture as a model system. It explores how intermolecular interactions and molecular size affect azeotropic behavior, and how these factors influence the shift in the azeotropic point.

The study is then extended to a real system by analyzing the VLE of a benzene–methanol azeotrope using the AMOEBA[21] force field, providing a more realistic perspective on the observed behavior..

2 Methodology

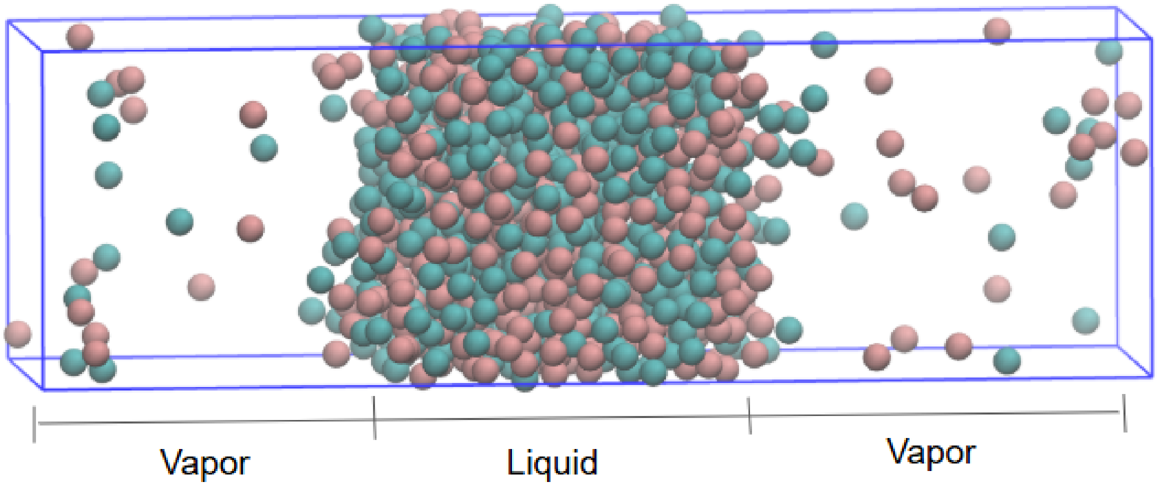

Figure 2: Schematic representation of vapor-liquid equilibrium.

2.1 Molecular Dynamics

Molecular Dynamics (MD)[22] simulation is employed in this study as a robust computational technique to investigate the microscopic behavior of the system. All simulations are performed using the GROMACS software[23] package, which enables efficient integration of Newton's equations of motion to model the time evolution of interacting particles. By updating particle positions and velocities over very small time intervals, the method produces a time-dependent trajectory of the system. Thermodynamic conditions, such as constant temperature or pressure, can be maintained using suitable control algorithms. From the generated trajectories, structural and dynamic properties including energy, pressure, and diffusion behavior, can be evaluated. Thus, molecular dynamics serves as an effective tool for connecting molecular-level interactions with the macroscopic properties observed in simulations.

2.2 Lennard Jones Model

The Lennard-Jones (LJ) potential is a simple mathematical model that describes how two neutral particles interact with each other depending on how far apart they are. It captures both the repulsive force when particles get too close and the attractive force when they are a bit farther apart.[24] [25] LJ potential can be calculated using the equation 6:

$$V(r) = 4\epsilon\left[\left(\frac{\sigma}{r}\right)^{12} - \left(\frac{\sigma}{r}\right)^{6}\right] \tag{6}$$

where V(r) is the potential energy between two particles separated by a distance r, ϵ represents the interaction strength between the particles and σ is the distance at which the potential energy between two particles becomes zero.

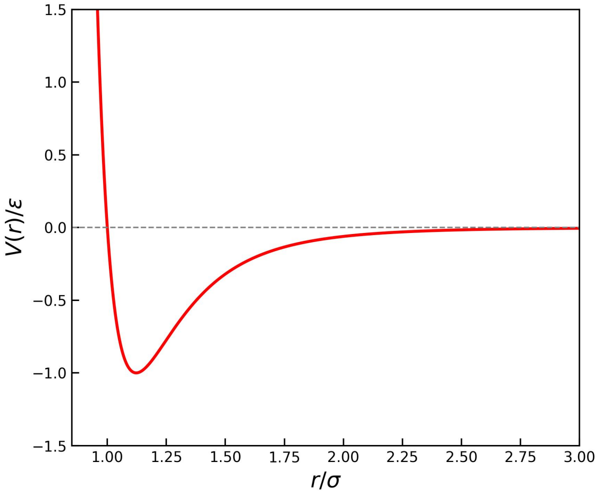

Figure 3: Lennard–Jones potential describes intermolecular interactions.

In molecular simulations, simple fluids and their mixtures are often modeled using the Lennard–Jones (LJ) potential due to its ability to capture short-range repulsive and long-range attractive interactions. When more than one molecular species is present, the system is referred to as a Lennard–Jones mixture. These mixtures can be classified as symmetric and asymmetric on the basis of similarity or disparity of the interaction parameters associated with different species.

A symmetric LJ mixture consists of two components with identical molecular sizes and interaction strengths. In this case, both species have the same LJ parameters for size (σ) and energy (ϵ), and the cross-interaction parameters are equal to those of the pure components.[26] In asymmetric LJ mixtures, the two components differ in size, interaction strength, or both.[27] This asymmetry introduces complexity into the system and leads to richer phase behavior compared to symmetric mixtures.

2.3 AMOEBA Model

The AMOEBA[21] [28] (Atomic Multipole Optimized Energetics for Biomolecular Applications) is a polarizable force field that describes molecular potential energy as the sum of bonded and non-bonded interactions. It extends the traditional classical force field formalism by incorporating explicit atomic multipoles and polarizability, allowing a more realistic representation of molecular electrostatics and intermolecular polarization effects.

The total potential energy in AMOEBA is written as the sum of bonded (valence) and non-bonded terms. The bonded interactions account for bond stretching, bond angle bending, torsional rotation, and out-of-plane bending, along with additional coupling terms such as π-torsion term, bond–angle coupling, and torsion–torsion couplings.[28] These terms enhance the accuracy of structural and vibrational property predictions in biomolecules.[29] Non-bonded interactions consist of van der Waals forces described by the buffered 14–7 potential[30] and permanent electrostatics represented by atomic multipoles (charge, dipole, and quadrupole moments). Polarization effects are treated explicitly using an induced dipole model,[31] [32] in which each atomic dipole responds to the electric field generated by all other permanent and induced multipoles.

A key strength of AMOEBA is its ability to include polarization effects, which means that atomic charges can adjust dynamically depending on their environment.[33] This makes it particularly effective for systems where hydrogen bonding and strong intermolecular interactions play an important role, such as in the benzene–methanol mixture. The force field also uses more flexible terms for bonded and van der Waals interactions, helping to reproduce molecular structures and physical properties with higher accuracy.

2.4 Simulation Details

2.4.1 Lennard Jones mixture

All the molecular dynamics simulations were done with GROMACS. We have simulated two types of systems, symmetric (single component) and asymmetric (σ or ϵ). Simulated a total of 1000 numbers of particles in different compositions and at different temperatures (60 K, 80 K, 100 K and 120 K).

In the **symmetric mixture**, all size (σ) and energy (ε) parameters are equal, so it behaves like a **single-component system** with identical self and cross interactions. In the **asymmetric (σ) case**, size parameters differ $(\sigma_{BB} > \sigma_{AB} > \sigma_{AA})$ while energy parameters remain the same, meaning particle sizes vary but interaction strength is equal. In the **asymmetric (ε) case**, energy parameters differ $(\varepsilon_{BB} > \varepsilon_{AB} > \varepsilon_{AA})$ while sizes are equal, indicating stronger self-interaction for B and intermediate cross interaction. .

Mixture	σ_{BB}/σ_{AA}	σ_{AB}/σ_{AA}	$\epsilon_{BB}/\epsilon_{AA}$	$\epsilon_{AB}/\epsilon_{AA}$
Symmetric	1.0	1.0	1.0	1.0
Asymmetric (σ)	1.15	1.075	1.0	1.0
Asymmetric (ϵ)	1.0	1.0	1.2	1.095

Table 1: Parameters for symmetric and asymmetric mixtures.

First, the steepest descent algorithm[34] was used to minimize energy to achieve a stable configuration in which the potential energy of the system was negative. After this, a 5 ns equilibration period (NVT) was performed, where a modified Berendsen thermostat[35] was used to slowly raise the system to the required temperatures. To enhance the mixing of the components, annealing was added with a time step of 0.001 ps. Then, a 5 ns period of equilibration (NPT) was performed. The Parrinello-Rahmann barostat[36][37] was used to equilibrate pressure, and all bond constraints were enforced with the LINCS algorithm.[38] Electrostatic calculations were performed using the particle Mesh Ewald (PME) method.[39]

This was followed by a production run (NPT) of 10 ns after equilibration. After that, we elongate the box dimension along the z-direction to 12 nm to form a liquid-vapor interface in that direction and run energy minimization and NVT equilibration for 20 ns to achieve vapor-liquid equilibrium. The last 10 ns of the 20 ns long simulation trajectories were used for analysis. Simulations of symmetric and asymmetric LJ mixtures were conducted in a wide range of compositions (χ_A = 0.1 to 0.9) in the temperature range between 60 K and 120 K. The systems were visualized with VMD,[40] and data analysis was conducted with the built-in GROMACS tools.

2.4.2 Benzene methanol binary mixture

Molecular simulations were performed using the TINKER software[41] in AMOEBA force field[21] for three systems: (i) 500 benzene molecules, (ii) 500 methanol molecules, and (iii) an azeotropic mixture of 300 methanol and 200 benzene molecules. Cubic simulation boxes of 43 Å, 33 Å, and 37 Å were used for benzene, methanol, and the mixture, respectively. Energy minimization was carried out using the L-BFGS algorithm method[42]. The systems were then sequentially equilibrated under NVT and NPT ensembles at 300 K and 1 atm. Molecular dynamics simulations were performed using the Beeman algorithm.[43]

3 Results and Discussion

3.1 Density Analysis

The number density profile describes how the particle density varies along the z-direction and is used to characterize interfacial behavior in molecular simulations. It is obtained by dividing the simulation box into thin slabs and calculating the average number of particles per unit volume in each slab.

3.1.1 Symmetric mixture

This figure (Figure 4) shows the number density profiles of component A along the z-direction for a symmetric mixture at different compositions and temperatures. At **low temperature (60 K)**, a highly ordered, **glassy-like structure** is observed in the liquid region. The **central flat region** (around $z \approx 4$–8 nm) represents the **liquid phase**, where the density is high and nearly constant. The **outer regions** (around $z \approx 0$–4 nm and 8–12 nm) correspond to the **vapor phase**, where the density is very low. The transition between these regions indicates the **interface**. As the **temperature increases**, the interface gradually becomes less sharp and more diffuse due to enhanced molecular motion. With higher **composition** (x_A), the liquid region becomes richer in component A, leading to an increase in its density, while the vapor phase remains relatively dilute. Overall, temperature influences the thickness of the interface, whereas composition primarily determines the liquid-phase density.

3.1.2 Asymmetric mixture (epsilon)

The plots (Figure 5) show the number density profiles of component A along the z-direction at different compositions $(x_A = 0.1$ to $0.9)$ and temperatures (60–120 K). The **central flat region** (around $z \approx 4$–8 nm) represents the **liquid phase**, where the density is high and nearly constant. The **outer regions** (around $z \approx 0$–4 nm and 8–12 nm) correspond to the **vapor phase**, where the density is very low. The transition between these regions indicates the **interface**. At **low temperature (60 K)**, a highly ordered, **glassy-like structure** is observed in the liquid region. As **temperature increases**, the interface becomes smoother and broader due to increased molecular motion. With increasing **composition** (x_A), the liquid-phase density of component A increases, while the vapor region remains

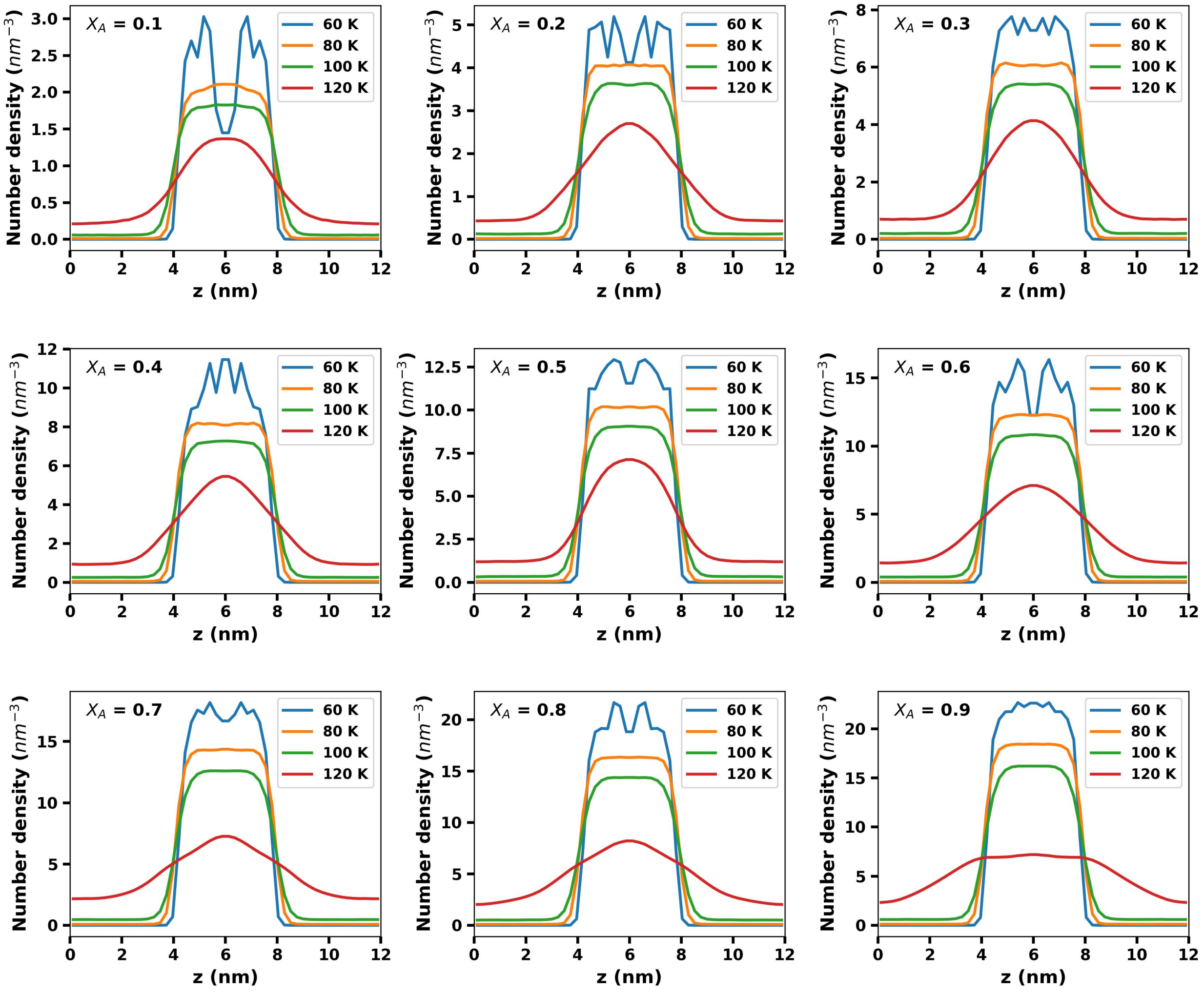

Figure 4: Number density profiles for symmetric mixture of component A along the z-direction at different compositions $(x_A = 0.1–0.9)$ and temperatures (60–120 K), highlighting the liquid region (high-density plateau), vapor region (low-density edges), and interfacial broadening with increasing temperature.

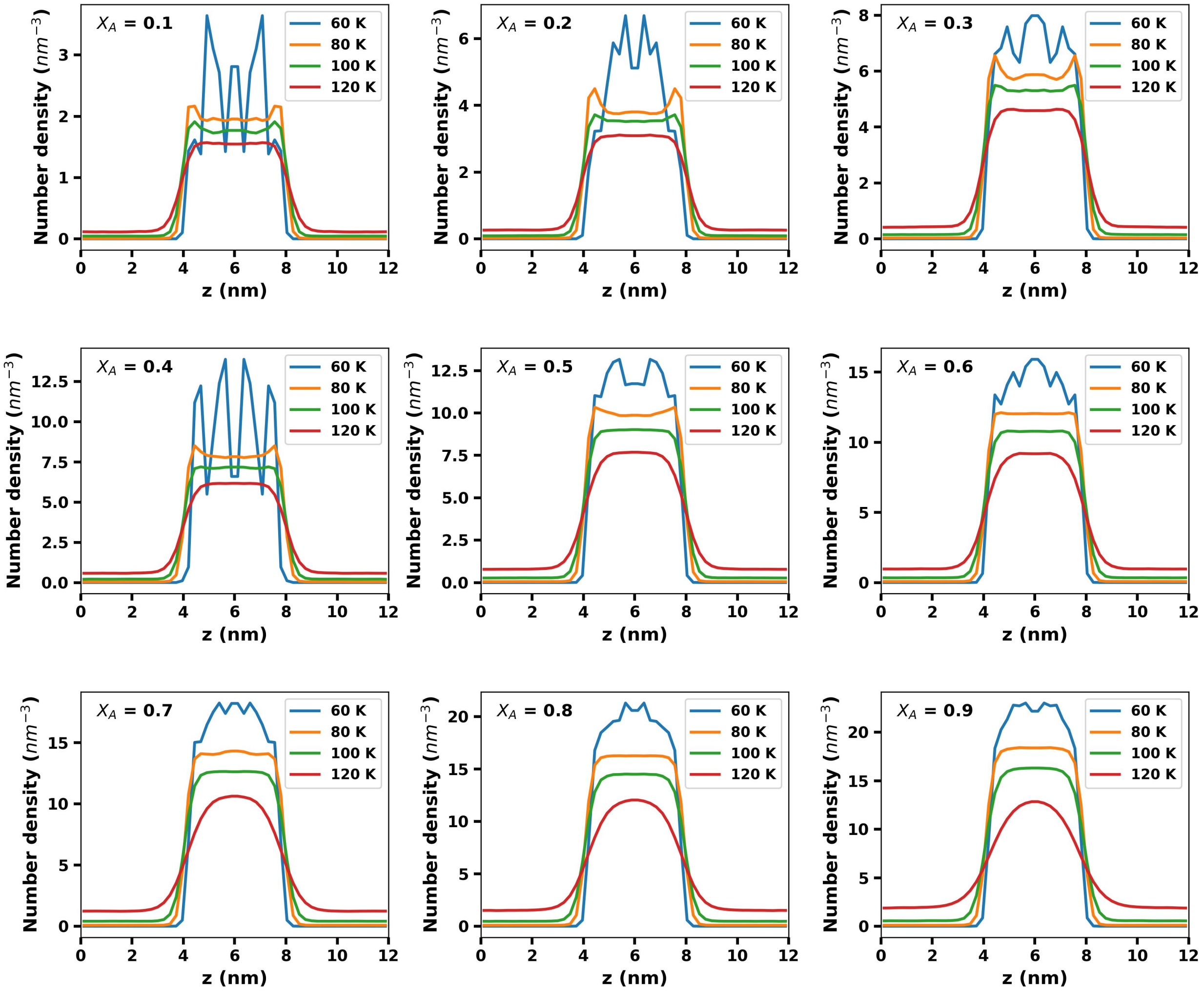

Figure 5: Number density profiles for asymmetric mixture (ϵ) of component A along the z-direction at different compositions $(x_A = 0.1–0.9)$ and temperatures (60–120 K), highlighting the liquid region (high-density plateau), vapor region (low-density edges), and interfacial broadening with increasing temperature.

dilute. Thus, temperature mainly affects interfacial thickness, whereas composition controls the liquid density.

3.1.3 Asymmetric mixture (sigma)

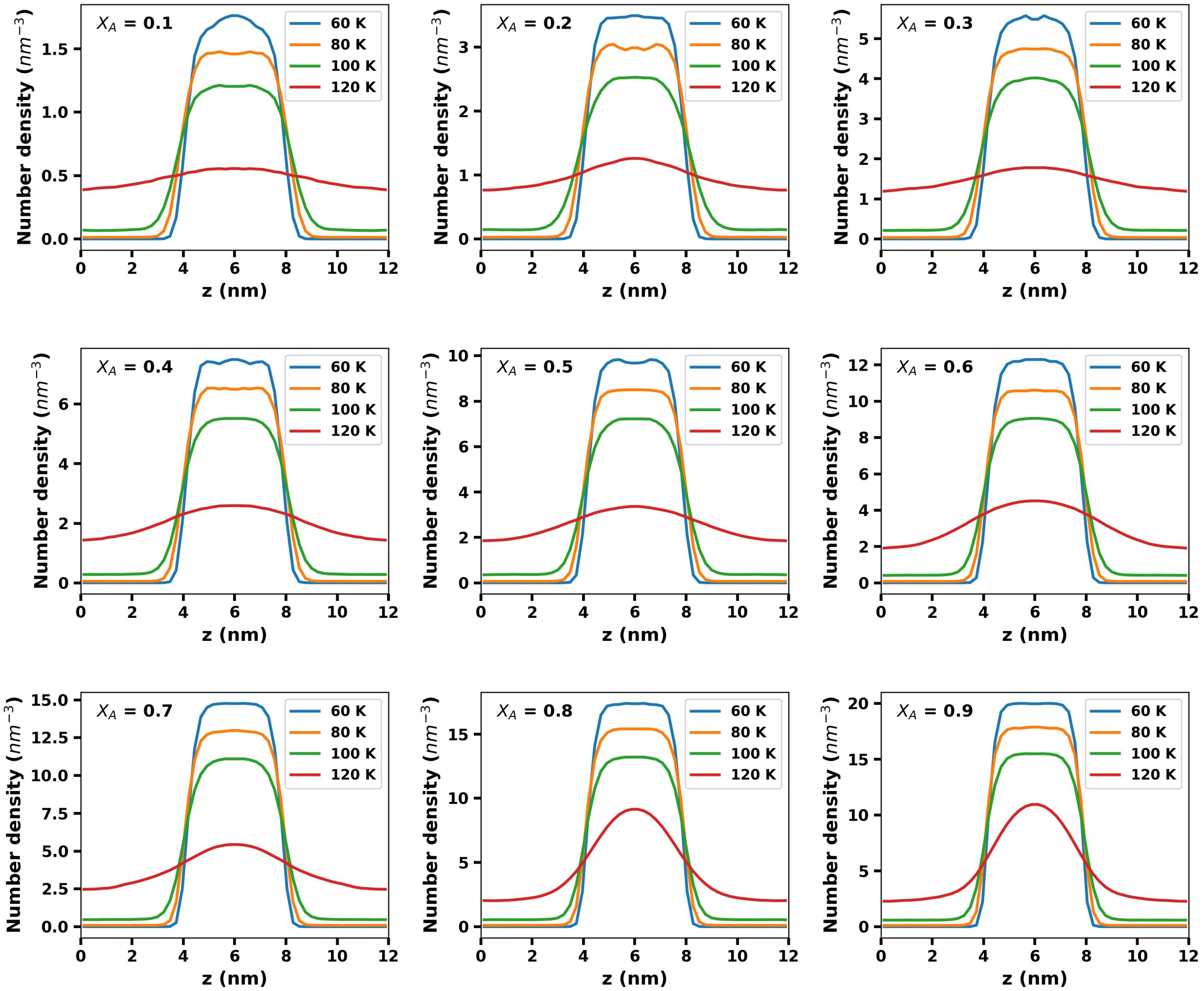

Figure 6: Number density profiles for asymmetric mixture (σ) of component A along the z-direction at different compositions $(x_A = 0.1–0.9)$ and temperatures (60–120 K), highlighting the liquid region (high-density plateau), vapor region (low-density edges), and interfacial broadening with increasing temperature.

This figure (Figure 6) shows the number density profiles of component A along the z-direction at different compositions and temperatures. At low temperature (60 K), a sharp high-density plateau (around $z \approx 4–8$ nm) in the center represents the liquid region, with low-density vapor regions (around $z \approx 0$–4 nm and 8–12 nm) on both sides. As temperature increases, the plateau height slightly decreases and the interface becomes broader due to increased molecular motion. Increasing composition (x_A) raises the overall density of A, making the liquid region more pronounced. Overall, temperature controls interfacial thickness, while composition affects density magnitude.

3.2 Radial Distribution Function (RDF)

The Radial Distribution Function (RDF)[44] was calculated to characterize the local structural organization and intermolecular interactions in the symmetric and asymmetric binary mixture. RDF was computed as shown in the equation 7 below :

$$g(r) = \frac{dN(r)}{4\pi r^2 \rho \, dr} \tag{7}$$

where ρ is the average number density, and $dN(r)$ is the average number of atoms located within a spherical shell of thickness dr at distance r from the reference atom.[44] In molecular dynamics simulations, the RDF is computed by dividing the simulation box into concentric spherical shells and averaging over all atomic pairs and time frames. When $g(r) = 1$, the system behaves like an ideal gas with random distribution. Values of $g(r) > 1$ indicate preferred interatomic distances and local structuring, while $g(r) < 1$ signifies regions of depletion.

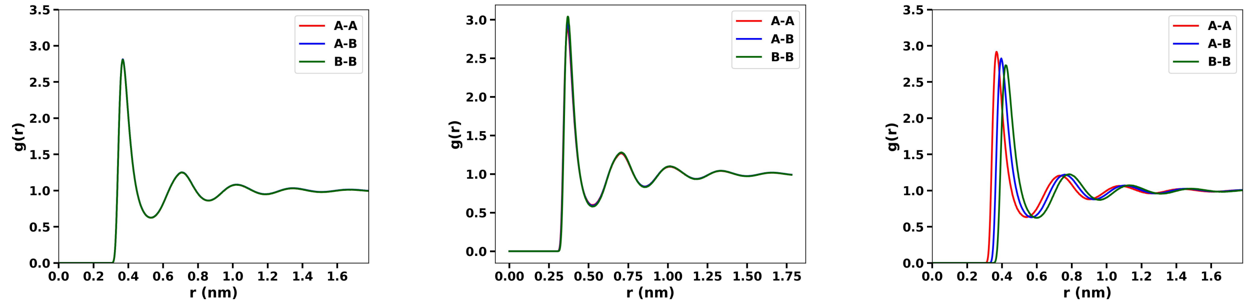

(a) (b) (c)

Figure 7: Radial distribution functions $g(r)$ for A–A, A–B, and B–B pairs for (a) symmetric, (b) ϵ-asymmetric, and (c) σ-asymmetric mixtures at $x_A = 0.5$ and $T = 100$ K, showing the variation in local structural ordering and intermolecular correlations.

3.2.1 Symmetric mixture

In the symmetric mixture (Figure 7a), all three RDF curves nearly overlap, indicating that the interactions between like and unlike pairs are similar (single component system). A sharp and well-defined first peak is observed at short distances (r $\approx$ 0.35 nm), corresponding to strong nearest-neighbor correlations and a high probability of finding surrounding particles at that separation. The absence of long-range order (local structural ordering decreases as moving to higher distance) confirms the characteristic liquid-like structure. The overlap of A–A, A–B and B–B curves suggests complete structural homogeneity in the system.

3.2.2 Asymmetric mixture (epsilon)

For the ϵ-asymmetric mixture (Figure 7b), where interaction strengths differ while molecular sizes remain unchanged, the RDF profiles retain similar peak positions compared to the symmetric case. This indicates that the average intermolecular distances are largely unaffected by variations in ϵ. However, noticeable differences in peak intensities are observed, particularly in the first coordination shell. The B–B interaction shows the highest first peak intensity, suggesting comparatively stronger self-association among B components than cross-interactions. Despite these variations, the overall structural pattern remains similar, suggesting that ϵ-asymmetry primarily influences the strength of correlations rather than the spatial arrangement.

3.2.3 Asymmetric mixture (sigma)

In contrast, the σ-asymmetric mixture (Figure 7c) shows significant deviations in both peak positions and intensities among the different interaction pairs. The first peak positions are clearly shifted, indicating changes in effective molecular diameters and nearest-neighbor distances. Specifically, interactions involving larger particles (B) exhibit peaks at greater separations, while smaller particles (A) show peaks at shorter distances. Additionally, the reduced overlap between A–A, A–B and B–B RDFs highlights increased structural heterogeneity and preferential packing effects.

Overall, the comparison reveals that ϵ-asymmetry mainly affects the magnitude of local structuring by modifying interaction strength, whereas σ-asymmetry has a more pronounced impact on both the spatial distribution and organization of molecules. This indicates that size disparity plays a dominant role in determining the microscopic structure of the mixture, leading to enhanced structural differentiation compared to energy asymmetry.

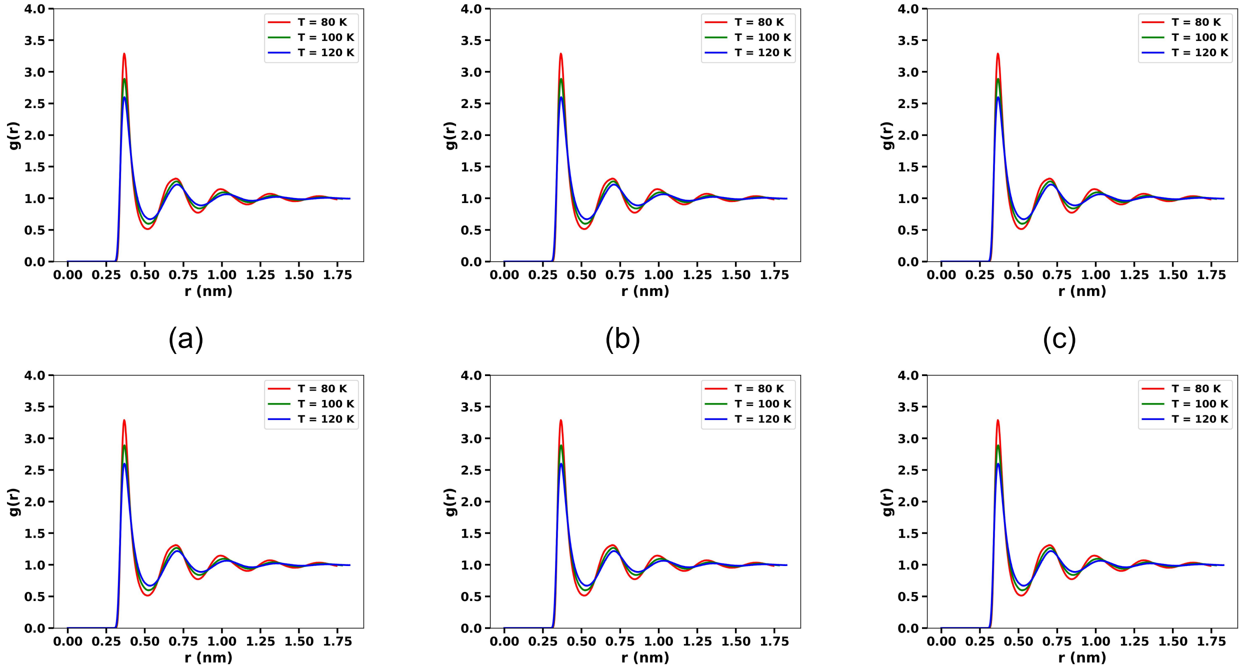

(a) (b) (c)

(d) (e) (f)

Figure 8: Temperature-dependent radial distribution functions $g(r)$ for A–A, A–B, and B–B pairs in asymmetric mixtures at $x_A = 0.5$. The first column represents A–A pairs, the second column A–B pairs, and the third column B–B pairs. The first row corresponds to ϵ-asymmetric mixtures, while the second row represents σ-asymmetric mixtures, illustrating the influence of interaction strength and particle size on local structural ordering.

Figure 8 shows the temperature-dependent radial distribution functions, $g(r)$, for A–A, A–B, and B–B pairs in ϵ- and σ-asymmetric mixtures at $x_A = 0.5$. A clear trend observed across all plots is that with increasing temperature, the height of the first and subsequent peaks decreases more rapidly this indicates a reduction in local structural ordering in both ϵ- and σ-asymmetric systems.

The decrease in ordering occurs because, at higher temperatures, particles possess greater thermal energy, which enhances their mobility and disrupts intermolecular interactions. As a result, the well-defined coordination shells observed at lower temperatures become less distinct, leading to a smoother $g(r)$ profile that gradually approaches unity. This behavior confirms that thermal motion weakens short-range correlations and reduces the degree of local structuring in the system.

3.3 Compositional Analysis

3.3.1 Symmetric mixture

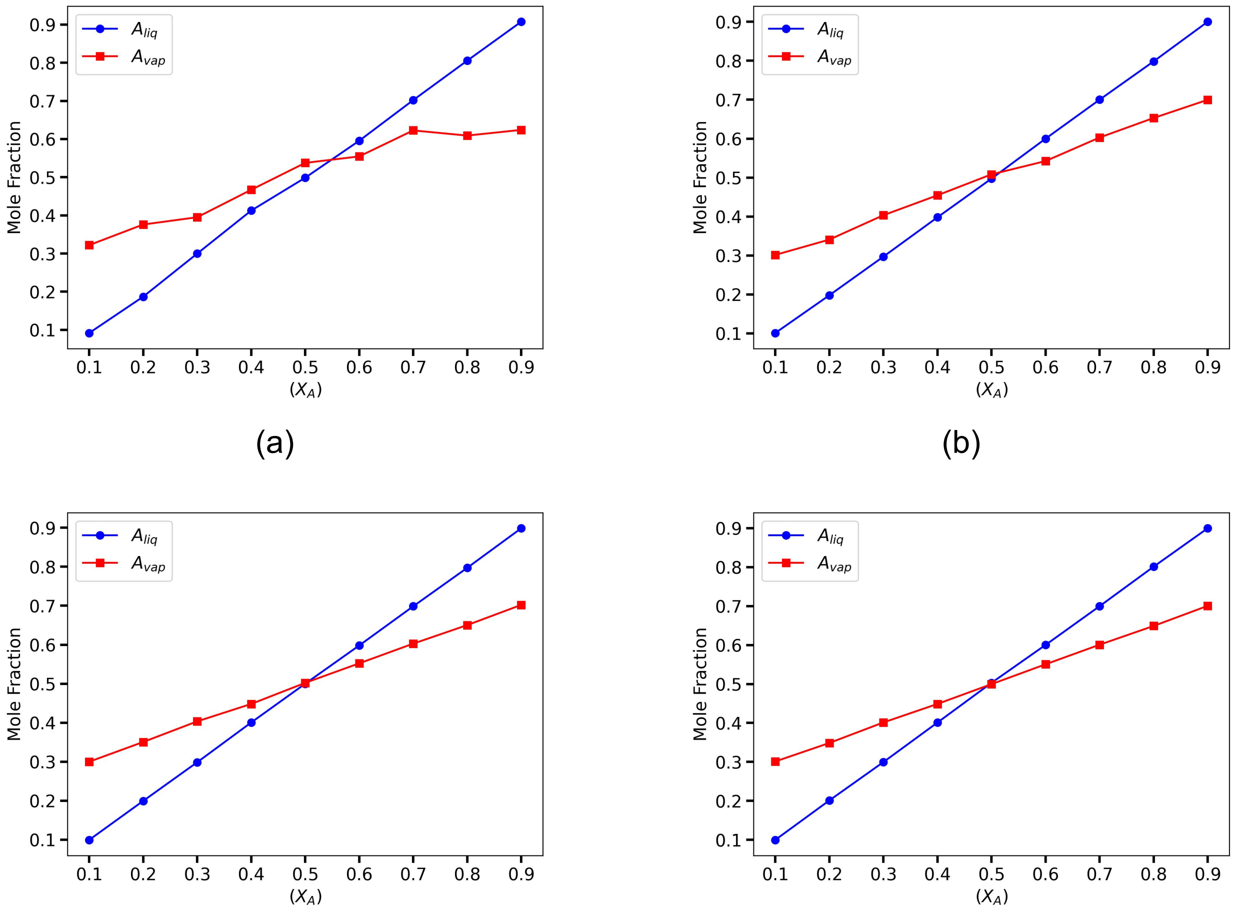

(a)

(b)

(c)

(d)

Figure 9: Composition variation of symmetric mixture (single component) at different temperatures (a) 60 K, (b) 80 K, (c) 100 K (d) 120 K.

Composition analysis plays a crucial role in understanding the phase behavior and thermodynamic properties of multi-component systems. It involves the quantitative determination of the distribution of individual components across different phases, such as liquid and vapor, under equilibrium conditions.

Figure 9 represents the composition profiles of the symmetric mixture (single component) at temperatures of 60 K, 80 K, 100 K and 120 K. These plots were used to compare with asymmetric mixtures. In each plot, the mole fraction of the liquid phase of component A increases linearly with the overall composition, whereas the mole fraction of the vapor phase varies more gradually. At 60 K, the curve of vapor composition of A is not smooth because of less sampling.

3.3.2 Asymmetric mixture (epsilon)

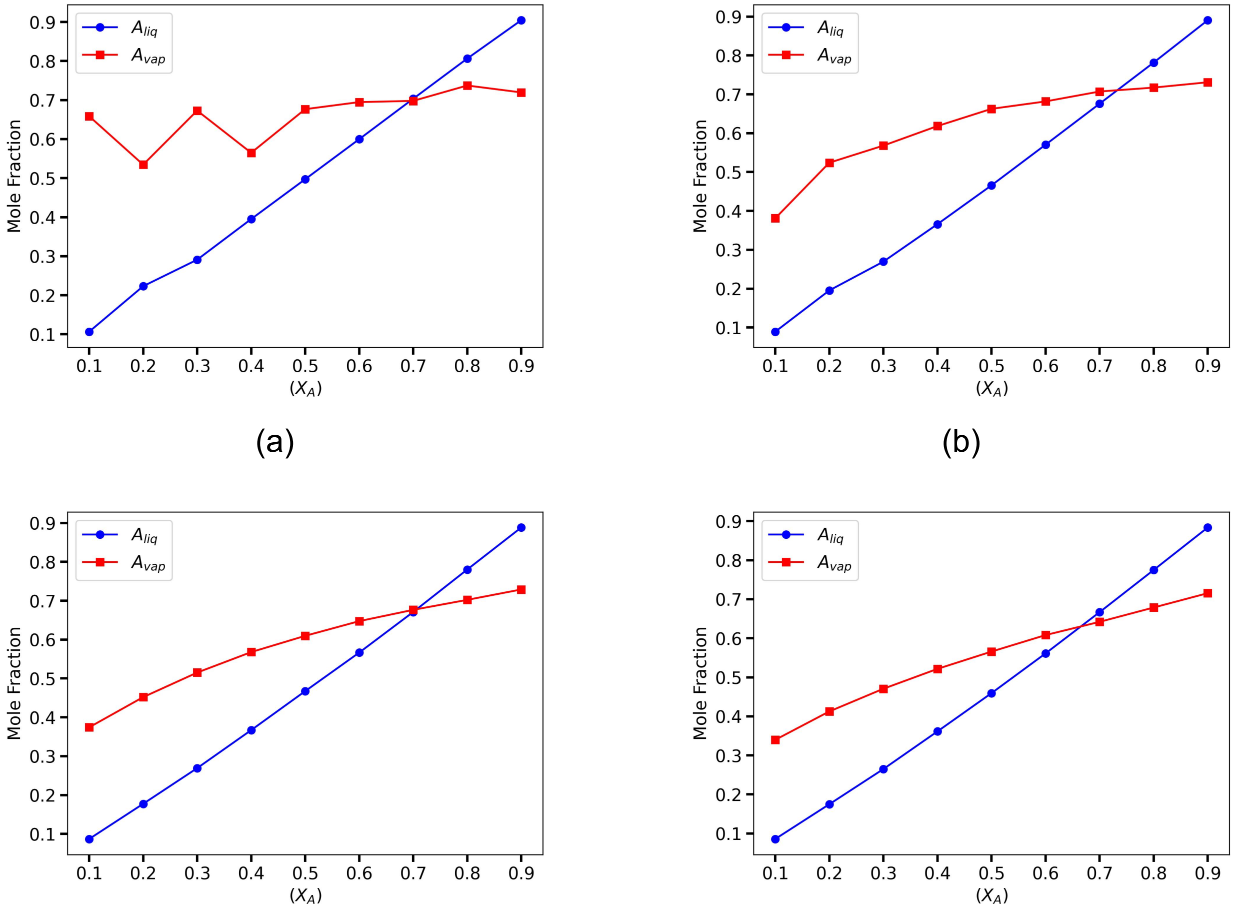

(a)

(b)

(c)

(d)

Figure 10: Composition variation of asymmetric (epsilon) mixture at different temperatures (a) 60 K, (b) 80 K, (c) 100 K (d) 120 K.

Figure 10 shows the behavior of the asymmetric mixture in equilibrium between the vapor and liquid at different temperatures. The curve of vapor composition (A_vap) at 60 K

(Fig. 10a) shows significant variations at lower mole fractions because of less sampling and crosses the curve of liquid composition (A_liq) at about $\chi_A \approx$ 0.70, indicating that there is an azeotropic composition. Further increasing the temperature to 80 K (Fig. 10b), the curve becomes smoother, and the azeotropic point moves slightly further to the higher composition, approximately $\chi_A \approx$ 0.75. At 100 K, the same trend is observed (Fig. 10c) with the azeotrope observed at or near $\chi_A \approx$ 0.72 with a more gradual change in vapor composition. At 120 K (Fig. 10d), the composition of the vapor-liquid is closer and the azeotropic point is shifted to $\chi_A \approx$ 0.68.

Compared to the symmetric mixture, the azeotropic point shifts toward a higher composition of component A. This shift occurs due to the relatively stronger interactions among component B molecules, which favor their retention in the liquid phase.

As a result, fewer B molecules escape into the vapor phase, leading to a decrease in the vapor-phase composition of B. Consequently, the vapor phase becomes richer in component A, causing the azeotropic composition to move toward higher x_A.

3.3.3 Asymmetric mixture (sigma)

Figure 11 shows the behavior of the vapor-liquid equilibrium of the asymmetric mixture at different temperatures. At 60 K (Fig. 11a), the curve of the vapor composition is seen to deviate significantly because of less sampling and crosses at $\chi_A \approx$ 0.35, indicating that an azeotropic composition will be present at a rather low mole fraction. When the temperature increases to 80 K (Fig. 11b), the curve of the vapor composition will be smoother, and the azeotropic point will shift to $\chi_A \approx$ 0.45. The point of intersection of two curves at 100 K (Fig. 11c) occurs near $\chi_A \approx$ 0.50, which indicates that the azeotrope shifts almost to an equimolar composition at higher temperature. The same was observed at 120 K (Fig. 11d), where the azeotropic composition is still around $\chi_A \approx$ 0.50.

Compared to the symmetric mixture, the azeotropic point shifts toward a lower composition of component A. This behavior arises due to the larger size of component B molecules, which creates a cage-like environment that traps A molecules within the liquid phase.

As a result, fewer A molecules escape into the vapor phase, leading to a reduced vapor-phase composition of A. Consequently, the azeotropic composition shifts toward lower values of x_A.

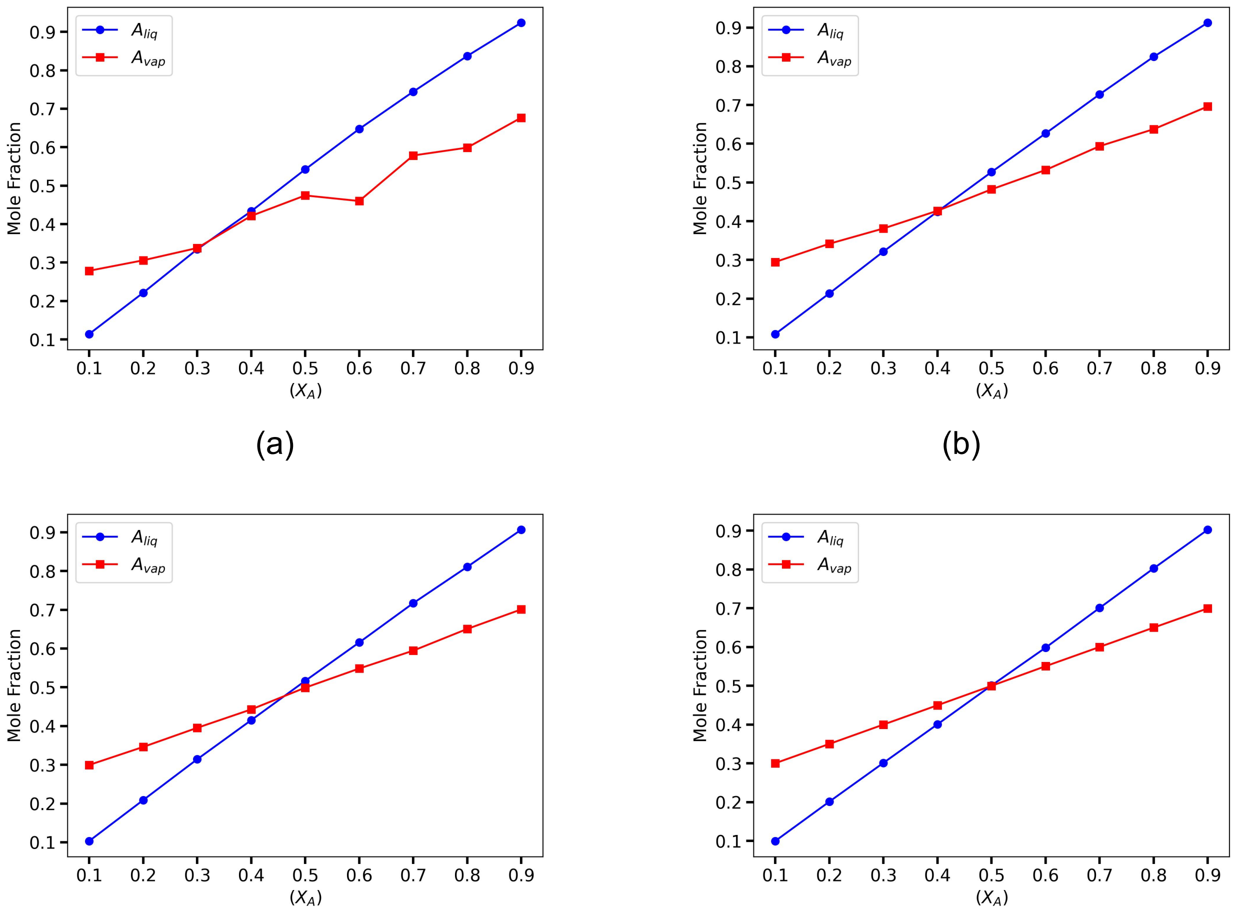

(a) (b)

(c) (d)

Figure 11: Composition variation of asymmetric (sigma) mixture at different temperatures (a) 60 K, (b) 80 K, (c) 100 K (d) 120 K.

3.4 Interfacial Analysis

The Pytim package[45] was employed to investigate the liquid–vapor interface using the ITIM (Identification of Truly Interfacial Molecules) algorithm[46]. In addition, custom Python scripts were developed using the MDAnalysis[47] library in conjunction with Pytim to compute the mole fraction of each component at the interface.

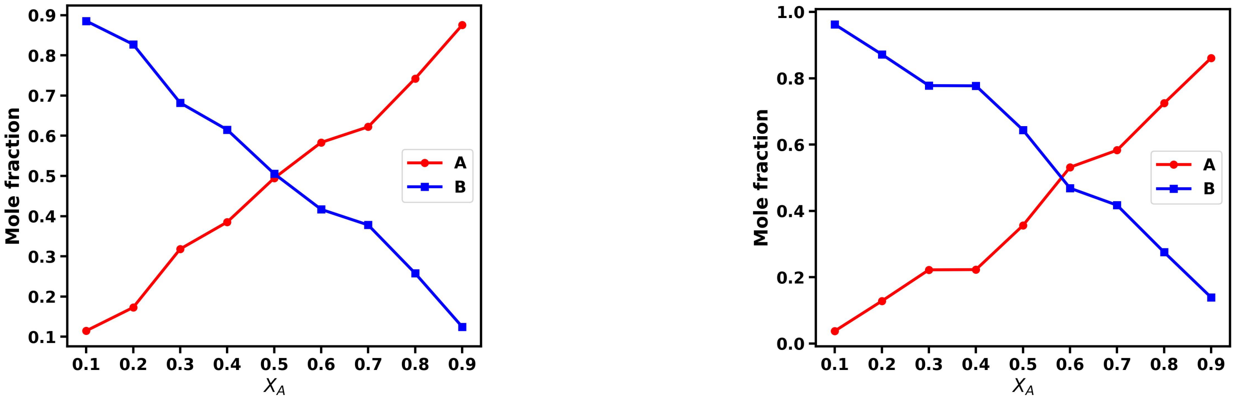

(a) Asymmetric (sigma)

(b) Asymmetric (epsilon)

Figure 12: Interfacial Composition of A and B at 100 K.

Figure 12 illustrates how the compositions of components A and B change across the interface under two different types of asymmetry, σ and ϵ. In both cases, as the mole fraction of A (x_A) increases, the amount of A gradually rises while B decreases in a complementary way, reflecting a natural redistribution of the two components across the interface.

In the σ-asymmetric case (Figure 12a), the transition is smooth and gradual. Around the composition $x_A \approx 0.5$, both A and B are present in nearly equal amounts. Moreover, if we equilibrate the system for longer time the mole fraction at the interface of both the compoenets becomes equal at the azeotropic composition.

In contrast, the ϵ-asymmetric case (Figure 12b) shows a relatively sharper transition. Here, the mole fraction of B decreases more quickly at higher values of x_A, suggesting a stronger tendency for separation. This behavior can be attributed to stronger B–B interactions, which make B molecules prefer to remain in the bulk liquid phase rather than at the interface. As a result, more A molecules accumulate at the interface, facilitating the transition from the liquid phase to the vapor phase. And if we equilibrate the system for longer time the mole fraction at the interface of both the components becomes equal at the azeotropic composition.

3.5 Results of AMOEBA

3.5.1 Density

Density is an important physical property for validating molecular simulations and the accuracy of the applied force field. Table 2 presents the experimental and simulated densities at 300 K for pure benzene, pure methanol, and the benzene–methanol azeotropic mixture. The simulated density in TraPPE-UA force field was used from previously reported results[48] to compare with the AMOEBA force field. The simulated density obtained using the AMOEBA force field is lower than the experimental and TraPPE-UA densities, implying a larger intermolecular separation and comparatively weaker molecular interactions. The simulated densities show a deviation of more than 8% from the experimental values for the pure components and 14.69% for the azeotropic mixture in the AMOEBA force field.

Liquid	Experimental	Simulated (AMOEBA)	Simulated (TraPPE-UA)
Benzene	868.2	792.5	870.1
Methanol	781.7	660.6	782.3
Azeotrope	840.0	716.6	793.7

Table 2: Experimental and Simulated Density (kg/m^3) for pure benzene and methanol at 300K.

3.5.2 Enthalpy of Vaporization

In molecular dynamics (MD) simulations, the enthalpy of vaporization serves as a crucial benchmark for assessing the accuracy of intermolecular interactions and, consequently, for validating the applied force field. It also plays a key role in predicting vapor–liquid equilibria, which are essential for designing efficient separation processes.

The enthalpy of vaporization was calculated using equation 8, where U_{gas} and U_{liquid} represent the potential energies of the gas and liquid phases, respectively, R is the universal gas constant and T is the temperature.[49]

$$\Delta H_{\text{vap}} = \langle U_{\text{gas}} \rangle - \langle U_{\text{liq}} \rangle + RT \tag{8}$$

Table 3 presents the values of the enthalpy of vaporization ($\Delta\ H_{\text{vap}}$) for pure benzene and methanol. The simulated enthalpy of vaporization in TraPPE-UA force field was used from previously reported results[48] to compare with AMOEBA force field. Compared to the experimental data and TraPPE-UA simulations, the AMOEBA model predicts a lower enthalpy of vaporization. This behavior correlates well with the density, indicating weaker intermolecular interactions and consequently lower energy requirements for phase transition. The simulated results show deviations of more than 25% from the corresponding experimental data, which does not indicate good agreement with the AMOEBA force field.

Liquid	Experimental	Simulated (AMOEBA)	Simulated (TraPPE-UA)
Benzene	30.70	13.91	39.62
Methanol	37.43	27.12	39.41

Table 3: Experimental and Simulated enthalpy of vaporisation (KJ/mol) for pure benzene and methanol.

3.5.3 Radial Distribution Function

Pure Benzene (C-C): Figure 13a presents the radial distribution function (RDF) of a pair of carbon-carbon (C–C) atoms in pure benzene, obtained using the AMOEBA and TraPPE-UA force field. In the AMOEBA simulation, the g(r) value remains close to zero up to about 2.5 Å, which means that no carbon atoms come closer than that distance. After this point, g(r) increases sharply and reaches a strong first peak around 5 Å. This peak represents the nearest-neighbor C–C interactions. Beyond approximately 10 Å, the g(r) value levels off at 1, indicating that the molecules are randomly distributed at longer distances. Compared with the TraPPE-UA force field, both models give very similar RDF curves. The positions of the peaks are nearly identical, indicating that both force fields describe the structure of liquid benzene well.

Pure Methanol (O-O): Figure 13b shows the RDF of a pair of carbon-carbon (C–C) atoms in pure methanol using the AMOEBA and TraPPE-UA force field. The sharp first peak at r $\approx$ 2.8 Å arises from strong hydrogen-bonding interactions between methanol molecules.

Benzene Methanol Azeotropic Mixture (C-C) and (O-O): Figure 13c shows the radial distribution function (RDF) for a pair of carbon-carbon (C–C) atoms of methanol molecules in the benzene–methanol mixture using AMOEBA and TraPPE-UA force field. However, we cannot conclude any interpretation from this graph. Figure 13d shows the radial distribution function (RDF) for a pair of oxygen–oxygen (O–O) atoms of methanol molecules in the benzene–methanol mixture using the AMOEBA and TraPPE-UA force field. The first

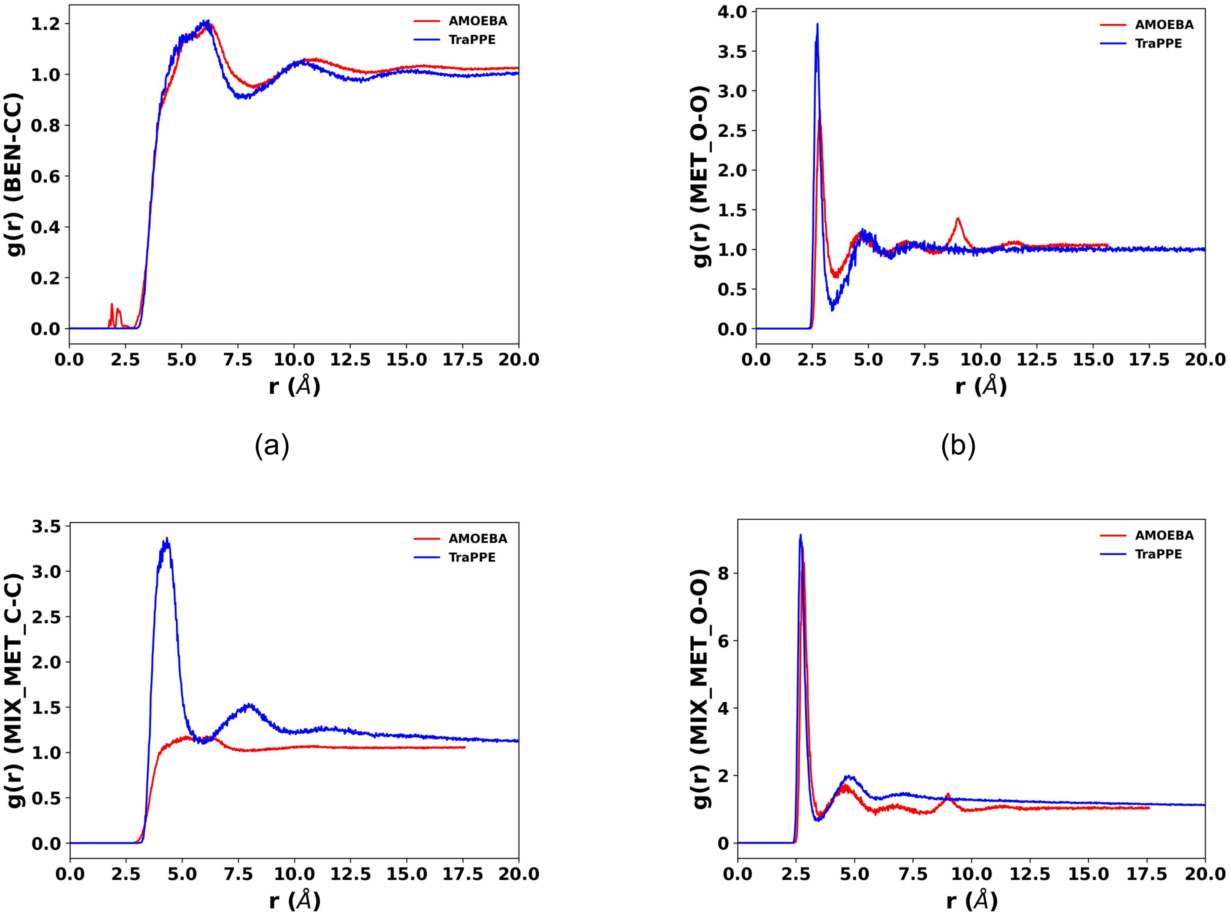

(a) (b)

(c) (d)

Figure 13: Radial distribution functions for selected atom pairs, comparing AMOEBA and TraPPE-UA force fields.

peak appears around r $\approx$ 2.8 Å for both force fields, corresponding to strong hydrogen-bonding interactions between methanol molecules.

4 Conclusion

This study aims to understand the effect of interactions and size on azeotropic behavior. And study the shift in the azeotropic point with changes in size and interactions.The simulations were carried out in a wide range of compositions (χ_A = 0.1 to 0.9) and temperatures (60 K, 80 K, 100 K and 120 K). The symmetric mixture (single component) and the asymmetric mixture were studied, in which the parameters of the intermolecular interactions epsilon(ϵ) and sigma(σ) changed to see how the intermolecular interactions influence the azeotropic behavior.

The profiles of number density clearly indicated the presence of the vapor and liquid regions and changed systematically with composition and temperature. Greater density variations and more distinct structural features appeared at lower temperatures with increased temperature, leading to a smooth distribution of densities as molecular motion increased. The radial distribution functions showed that there was short-range order near the liquid phase, and the intensities of the peaks decreased with temperature. A composition analysis showed that there was a steady correlation between the total mole fraction and the concentration of each component contained in the system. In addition, interface analysis conducted on the asymmetric systems revealed that the mole fraction at the interface of both components will become equal at the azeotropic composition, if we equilibrate for longer time. In single line we can conclude that “The azeotropic behavior is strongly affected by interaction asymmetry”.

Simulations of the benzene–methanol azeotropic system were also performed using the AMOEBA force field; however, reliable results could not be obtained due to difficulties in achieving stable pressure equilibration. In future work, more advanced machine learning potentials will be explored to improve the accuracy and efficiency of the molecular simulations.

In conclusion, the findings are useful for understanding the effects of temperature, composition, and asymmetry of interaction and molecular size of Lennard-Jones mixtures. The findings are useful in improving the knowledge of the molecular interactions that regulate the equilibrium of the vapor and liquid in model fluid systems. And also important for improving separation process in phsyical chemistry.

References

[1] Manjul Yadav. Calculation of vapor–liquid phase diagram of the binary mixture of methanol and benzene using gibbs ensemble monte carlo. Bs-ms thesis, Indian Institute of Science Education and Research Pune, Pune, India, December 2021.

[2] Yaşar Demirel. 1 - fundamentals of equilibrium thermodynamics. In Yaşar Demirel, editor, *Nonequilibrium Thermodynamics (Second Edition)*, pages 1–52. Elsevier Science B.V., Amsterdam, second edition edition, 2007.

[3] Soemantri Widagdo and Warren D Seider. Journal review. azeotropic distillation. *AIChE Journal*, 42(1):96–130, 1996.

[4] Zhigang Lei, Chengyue Li, and Biaohua Chen. Extractive distillation: a review. *Separation & Purification Reviews*, 32(2):121–213, 2003.

[5] Shisheng Liang, Yujuan Cao, Xingzhen Liu, Xin Li, Yongteng Zhao, Yongkun Wang, and Yinglong Wang. Insight into pressure-swing distillation from azeotropic phenomenon to dynamic control. *Chemical Engineering Research and Design*, 117:318–335, 2017.

[6] William L Luyben and I-Lung Chien. *Design and control of distillation systems for separating azeotropes*. John Wiley & Sons, 2011.

[7] Federica Valentini and Luigi Vaccaro. Azeotropes as powerful tool for waste minimization in industry and chemical processes. *Molecules*, 25(22):5264, 2020.

[8] Saeid Aghahossein Shirazi, Bahareh Abdollahipoor, Bret Windom, Kenneth F Reardon, and Thomas D Foust. Effects of blending c3-c4 alcohols on motor gasoline properties and performance of spark ignition engines: A review. *Fuel processing technology*, 197:106194, 2020.

[9] Akshay Loyte, Jiwak Suryawanshi, Girish Bhiogade, Yuvarajan Devarajan, and Ganesan Subbiah. Recent developments in utilizing hydrous ethanol for diverse engine technologies. *Chemical Engineering and Processing-Process Intensification*, 177:108985, 2022.

[10] Barbara Kanegsberg and Edward Kanegsberg. *Handbook for critical cleaning: cleaning agents and systems*. CRC press, 2011.

[11] Darren L Williams. Development of azeotropic blends to replace tce and npb in vapor degreasing operations. Technical report, 2016.

[12] Dongyang Li, Ziqi Gao, Naveen Kumar Vasudevan, Hong Li, Xin Gao, Xingang Li, and Li Xi. Molecular mechanism for azeotrope formation in ethanol/benzene binary mixtures through gibbs ensemble monte carlo simulation. *The Journal of Physical Chemistry B*, 124(16):3371–3386, 2020. PMID: 32250637.

[13] Dario Camuffo. Chapter 4 - consequences of the maxwell–boltzmann distribution. In Dario Camuffo, editor, *Microclimate for Cultural Heritage (Third Edition)*, pages 61–71. Elsevier, third edition edition, 2019.

[14] Yoshikata Koga. Chapter ii - solution thermodynamics—use of the second and third derivatives of g. In Yoshikata Koga, editor, *Solution Thermodynamics and its Application to Aqueous Solutions (Second Edition)*, pages 27–61. Elsevier, second edition edition, 2017.

[15] Thomas A Halgren and Wolfgang Damm. Polarizable force fields. *Current Opinion in Structural Biology*, 11(2):236–242, 2001.

[16] William L Jorgensen, David S Maxwell, and Julian Tirado-Rives. Development and testing of the opls all-atom force field on conformational energetics and properties of organic liquids. *Journal of the american chemical society*, 118(45):11225–11236, 1996.

[17] Alex D MacKerell Jr, Donald Bashford, MLDR Bellott, Roland Leslie Dunbrack Jr, Jeffrey D Evanseck, Martin J Field, Stefan Fischer, Jiali Gao, Houyang Guo, Sookhee Ha, et al. All-atom empirical potential for molecular modeling and dynamics studies of proteins. *The journal of physical chemistry B*, 102(18):3586–3616, 1998.

[18] Junmei Wang, Piotr Cieplak, and Peter A Kollman. How well does a restrained electrostatic potential (resp) model perform in calculating conformational energies of organic and biological molecules? *Journal of computational chemistry*, 21(12):1049–1074, 2000.

[19] Walter RP Scott, Philippe H Hünenberger, Ilario G Tironi, Alan E Mark, Salomon R Billeter, Jens Fennen, Andrew E Torda, Thomas Huber, Peter Krüger, and Wilfred F Van Gunsteren. The gromos biomolecular simulation program package. *The Journal of Physical Chemistry A*, 103(19):3596–3607, 1999.

[20] Bin Chen, Jeffrey J Potoff, and J Ilja Siepmann. Monte carlo calculations for alcohols and their mixtures with alkanes. transferable potentials for phase equilibria. 5. united-atom description of primary, secondary, and tertiary alcohols. *The Journal of Physical Chemistry B*, 105(15):3093–3104, 2001.

[21] Jay W. Ponder, Chuanjie Wu, Pengyu Ren, Vijay S. Pande, John D. Chodera, Michael J. Schnieders, Imran Haque, David L. Mobley, Daniel S. Lambrecht, Robert A. Jr. DiStasio, Martin Head-Gordon, Gary N. I. Clark, Margaret E. Johnson, and Teresa Head-Gordon. Current status of the amoeba polarizable force field. *The Journal of Physical Chemistry B*, 114(8):2549–2564, 2010. PMID: 20136072.

[22] Daan Frenkel and Berend Smit. Chapter 4 - molecular dynamics simulations. In Daan Frenkel and Berend Smit, editors, *Understanding Molecular Simulation (Third Edition)*, pages 97–124. Academic Press, third edition edition, 2023.

[23] David Van Der Spoel, Erik Lindahl, Berk Hess, Gerrit Groenhof, Alan E Mark, and Herman JC Berendsen. Gromacs: fast, flexible, and free. *Journal of computational chemistry*, 26(16):1701–1718, 2005.

[24] Xipeng Wang, Simón Ramírez-Hinestrosa, Jure Dobnikar, and Daan Frenkel. The lennard-jones potential: when (not) to use it. *Phys. Chem. Chem. Phys.*, 22:10624–10633, 2020.

[25] Peter Schwerdtfeger and David J. Wales. 100 years of the lennard-jones potential. *Journal of Chemical Theory and Computation*, 20(9):3379–3405, 2024. PMID: 38669689.

[26] Ivan Antolović, Jens Staubach, Simon Stephan, and Jadran Vrabec. Phase equilibria of symmetric lennard-jones mixtures and a look at the transport properties near the upper critical solution temperature. *Phys. Chem. Chem. Phys.*, 25:17627–17638, 2023.

[27] Sergey P. Protsenko and Vladimir G. Baidakov. Binary lennard-jones mixtures with highly asymmetric interactions of the components. 1. effect of the energy parameters on phase equilibria and properties of liquid-gas interfaces. *Fluid Phase Equilibria*, 429:242–253, 2016.

[28] Brandon Walker, Chengwen Liu, Elizabeth Wait, and Pengyu Ren. Automation of amoeba polarizable force field for small molecules: Poltype 2. *Journal of Computational Chemistry*, 43(23):1530–1542, 2022.

[29] Yu-Chun Lin, Pengyu Ren, and Lauren J. Webb. Amoeba force field trajectories improve predictions of accurate pka values of the gfp fluorophore: The importance of polarizability and water interactions. *The Journal of Physical Chemistry B*, 126(40):7806–7817, 2022. PMID: 36194474.

[30] Thomas A Halgren. The representation of van der waals (vdw) interactions in molecular mechanics force fields: potential form, combination rules, and vdw parameters. *Journal of the American Chemical Society*, 114(20):7827–7843, 1992.

[31] Erle C. Donaldson and Waqi Alam. Chapter 2 - surface forces. In Erle C. Donaldson and Waqi Alam, editors, *Wettability*, pages 57–119. Gulf Publishing Company, 2008.

[32] Jacob N. Israelachvili. 5 - interactions involving the polarization of molecules. In Jacob N. Israelachvili, editor, *Intermolecular and Surface Forces (Third Edition)*, pages 91–106. Academic Press, San Diego, third edition edition, 2011.

[33] Modesto Orozco and Francisco J. Luque. Generalization of the molecular electrostatic potential for the study of noncovalent interactions. In Jane S. Murray and Kalidas Sen, editors, *Molecular Electrostatic Potentials*, volume 3 of *Theoretical and Computational Chemistry*, pages 181–218. Elsevier, 1996.

[34] William Press, S. Teukolsky, William Vetterling, and Brian Flannery. Book review: Numerical recipes in fortran: the art of scientific computing / cambridge u press. *The Observatory*, 113:214, 07 1993.

[35] Giovanni Bussi, Davide Donadio, and Michele Parrinello. Canonical sampling through velocity rescaling. *The Journal of chemical physics*, 126:014101, 02 2007.

[36] M. Parrinello and A. Rahman. Polymorphic transitions in single crystals: A new molecular dynamics method. *Journal of Applied Physics*, 52(12):7182–7190, 12 1981.

[37] Shuichi Nosé and Michael L. Klein. Constant pressure molecular dynamics for molecular systems. *Molecular Physics*, 50:1055–1076, 1983.

[38] Berk Hess, Henk Bekker, Herman J. C. Berendsen, and Johannes G. E. M. Fraaije. Lincs: A linear constraint solver for molecular simulations. *Journal of Computational Chemistry*, 18(12):1463–1472, 1997.

[39] Tom Darden, Darrin York, and Lee Pedersen. Particle mesh ewald: An n·log(n) method for ewald sums in large systems. *The Journal of Chemical Physics*, 98(12):10089–10092, 1993.

[40] William Humphrey, Andrew Dalke, and Klaus Schulten. Vmd: visual molecular dynamics. *Journal of molecular graphics*, 14(1):33–38, 1996.

[41] Joshua A. Rackers, Zhi Wang, Chao Lu, Marie L. Laury, Louis Lagardère, Michael J. Schnieders, Jean-Philip Piquemal, Pengyu Ren, and Jay W. Ponder. Tinker 8: Software Tools for Molecular Design. *Journal of Chemical Theory and Computation*, 14(10):5273–5289, October 2018.

[42] Yunhai Xiao, Zengxin Wei, and Zhiguo Wang. A limited memory bfgs-type method for large-scale unconstrained optimization. *Computers Mathematics with Applications*, 56(4):1001–1009, 2008.

[43] M. Amini, J.W. Eastwood, and R.W. Hockney. Time integration in particle models. *Computer Physics Communications*, 44(1):83–93, 1987.

[44] Elaheh K. Goharshadi. A review on the radial distribution function: Insights into molecular structure, intermolecular interactions, and thermodynamic properties. *Journal of Molecular Liquids*, 433:127900, 2025.

[45] Marcello Sega, György Hantal, Balázs Fábián, and Pál Jedlovszky. Pytim: A python package for the interfacial analysis of molecular simulations, 2018.

[46] Lívia B Pártay, György Hantal, Pál Jedlovszky, Árpád Vincze, and George Horvai. A new method for determining the interfacial molecules and characterizing the surface roughness in computer simulations. application to the liquid–vapor interface of water. *Journal of computational chemistry*, 29(6):945–956, 2008.

[47] Naveen Michaud-Agrawal, Elizabeth J Denning, Thomas B Woolf, and Oliver Beckstein. Mdanalysis: a toolkit for the analysis of molecular dynamics simulations. *Journal of computational chemistry*, 32(10):2319–2327, 2011.

[48] Parth Joshi, Manjul Yadav, and Arnab Mukherjee. Computational investigation of benzene-methanol azeotrope: Insights from molecular dynamics and monte carlo simulations. *ChemRxiv*, 2025(1021), 2025.

[49] Anjali Gaur and Sundaram Balasubramanian. Liquid–vapor interface of aqueous ethylene glycol solutions: A molecular dynamics study. *Langmuir*, 40(1):230–240, 2023.